GEOPHYSICS, VOL. 56, NO. 2 (FEBRUARY 1991); P. 168–181, 10 FIGS.

Interface conditions for acoustic and elastic wave propagation

J. S. Sochacki*, J. H. George*, R. E. Ewing*, and S. B. Smithson‡

ABSTRACT

The divergence theorem is used to handle the physics required at interfaces for acoustic and elastic wave propagation in heterogeneous media. The physics required at regular and irregular interfaces is incorporated into numerical schemes by integrating across the interface. The technique, which can be used with many numerical schemes, is applied to finite differences.

A derivation of the acoustic wave equation, which is readily handled by this integration scheme, is outlined. Since this form of the equation is equivalent to the scalar *SH* wave equation, the scheme can be applied to this equation also. Each component of the elastic *P-SV* equation is presented in divergence form to apply this integration scheme, naturally incorporating the continuity of the normal and tangential stresses required at regular and irregular interfaces.

INTRODUCTION

One of the difficult, yet interesting, problems in dealing with the earth's interior is that it is a complicated heterogeneous medium in which the physical parameters change continuously, randomly, or abruptly along regular or irregular boundaries. In this paper, we consider the problem of obtaining synthetic seismograms using the acoustic and elastic wave equations in regions containing regular and irregular boundaries or interfaces. Many successful techniques for handling different types of heterogeneities have been developed. We consider a technique that is not entirely new (see Mitchell, 1969) but to our knowledge has not yet appeared in the seismic literature. The technique handles the physics required at interfaces but can also treat variable parameters effectively.

One possible technique in the context of interface problems is to write the scalar and elastic wave equations as a system of first-order hyperbolic equations. This technique, which uses a staggered grid, was introduced by Madariaga (1976) in studying a circular fault. Virieux (1984, 1986) used the technique on the elastic *SH* and elastic *P-SV* equations and obtained nice results for difficult situations. Levander (1988) improved the accuracy of this scheme by using fourth-order differences in space. A second method, presented by Kummer and Behle (1982) and also considered by Kelly et al. (1976), is to use the physical boundary conditions explicitly at the interface. The method which we improve upon is outlined in Mitchell (1969) and used by Kelly et al. (1976, 1982) and Boore (1972). The fundamental concept is to integrate the acoustic and elastic wave equations across the interfaces.

We consider the method in a different way and obtain some better and interesting results. Our codes use explicit finite-difference schemes which easily incorporate integration; they also do not increase memory allocation requirements. Expressing the acoustic and elastic wave equations as first-order systems increases the number of vectors and, therefore, memory requirements. These systems actually solve for the velocities of the quantities needed. Dougherty and Stephen (1988) expressed the vector elastic wave equations as a second-order system to save memory and then apply the staggered-grid approach. However, we prefer to retain second-order equations because error estimates for approximating the physical boundary conditions are easily attained and the shape of the interfaces can be taken into account. Our schemes are comparable to Brown's (1984) system for a physical interface.

The acoustic equation is actually a first-order system for pressure and velocity; the equation that we consider is similar to the acoustic equation but is not common in the geophysical literature. We present the acoustic derivation, then we derive our equation and note interesting differences. The elastic equation is then written in divergence form so that it can be directly related to the technique derived for the acoustic equation.

One reason for this approach is that many geophysicists use the heterogeneous formulation of Kelly et al. (1976) even

Manuscript received by the Editor August 5, 1988; revised manuscript received August 16, 1990.
*Department of Mathematics, University of Wyoming, Box 3036, Laramie, WY 82071.
‡Department of Geology and Geophysics, University of Wyoming, Box 3006, Laramie, WY 82071.

though many investigators have noted problems with the scheme for complicated interfaces. The scheme presented here is based on forcing continuity of the appropriate physical quantities across interfaces and hence handles curved interfaces and incorporates the interface conditions more accurately. Stability can be maintained if the von Neumann stability criterion is preserved in each of the model's homogeneous regions.

The scheme is presented in detail for 1-D wave propagation with error analysis and comparison. A derivation of the acoustic wave equation is then given which leads to the general 2-D scalar wave equation. The scheme is presented for this equation, along with an outline for deriving error estimates. The Appendix details the scheme for some examples and includes error analysis. The numerical equations for approximating the elastic *P-SV* equations are then presented and an example is outlined. The example in the Appendix indicates how error estimates can be obtained.

THE EQUATIONS

Derivation of the acoustic equation

The system of equations used to model the propagation of sound waves in a medium is given by Landau and Lifshitz (1959) as

$$p_t + c^2\nabla\cdot(\rho_0\mathbf{v}) = 0, \qquad (a)$$
$$\mathbf{v}_t + \frac{1}{\rho_0}\nabla p = \mathbf{F}(\mathbf{x}, t), \quad (b) \qquad (1)$$

where p is the pressure, $\mathbf{v} = (v_1, v_2, v_3)$ is the velocity, ρ_0 is the equilibrium density, c is the speed of sound in the medium, and $\mathbf{F}(\mathbf{x}, t) = (F_1, F_2, F_3)$ is the external source at $\mathbf{x} = (x_1, x_2, x_3)$. If $\mathbf{n}$ is the unit normal to an interface in the medium, then the relevant physics requires that p and $\mathbf{v}\cdot\mathbf{n}$ be continuous at the interface.

Let u solve the wave equation

$$u_{tt} - c^2\nabla\cdot\nabla\mathbf{u} = g(\mathbf{x}, t); \qquad (2)$$

then let $p = -u_t$ and $\mathbf{v} = (1/\rho_0)\nabla\mathbf{u} + G$ where $g = c^2\nabla\cdot(\rho_0 G)$ and $G_t = F$, and note that p and $\mathbf{v}$ solve equation (1). We use equation (2) to solve for u to obtain the pressure. We use equation (2) because we want to incorporate the conditions that p and $\mathbf{v}\cdot\mathbf{n}$ be continuous at an interface in terms of a single variable and its normal derivative instead of having to use the system in equation (1). We show that the interface conditions in terms of u_t and $(1/\rho_0)\nabla\mathbf{u}\cdot\mathbf{n}$ are easily treated using equation (2).

We also note that the equation

$$\left(\frac{1}{\rho_0 c^2}\right)p_{tt} - \nabla\cdot\left(\frac{1}{\rho_0}\nabla p\right) = p_s(\mathbf{x}, t) \qquad (3)$$

is usually used to calculate the pressure. Equation (3) is obtained by dropping the term grad $\rho_0\cdot\mathbf{v}$ in equation (1.a), taking the time derivative of the remaining terms in equation (1.a) and the divergence of equation (1.b) and equating the two results. We use equation (2) to develop accurate approximations to the interface conditions because it can include the boundary conditions directly and because equation (3) does not explicitly contain the velocity; we use the form of equation (3) to derive our scheme. Since the source F is usually localized in exploration geophysics, we will ignore it when dealing globally with p and $\mathbf{v}$. [See Kelly et al. (1976) for methods for incorporating the source.]

The elastic *P-SV* equation

The 2-D elastic wave equation system used to model horizontal (u) and vertical (w) displacements in an isotropic medium is given by (Ewing et al., 1957)

$$\rho_0 u_{tt} = \frac{\partial}{\partial x}\left[(\lambda+2\mu)\frac{\partial u}{\partial x} + \lambda\frac{\partial w}{\partial z}\right] + \frac{\partial}{\partial z}\left[\mu\left(\frac{\partial u}{\partial z} + \frac{\partial w}{\partial x}\right)\right] + F_1(x, z, t)$$
$$\rho_0 w_{tt} = \frac{\partial}{\partial x}\left[\mu\left(\frac{\partial u}{\partial z} + \frac{\partial w}{\partial x}\right)\right] + \frac{\partial}{\partial z}\left[\lambda\frac{\partial u}{\partial x} + (\lambda+2\mu)\frac{\partial w}{\partial z}\right] + F_2(x, z, t), \qquad (4)$$

or

$$\rho_0 u_{tt} = \frac{\partial}{\partial x}(S_{xx}) + \frac{\partial}{\partial z}(S_{xz}) + F_1(x, z, t)$$
$$\rho_0 w_{tt} = \frac{\partial}{\partial x}(S_{zx}) + \frac{\partial}{\partial z}(S_{zz}) + F_2(x, z, t), \qquad (4a)$$

where λ and μ are the Lamé parameters, ρ_0 is the density, F_1 and F_2 are local sources, and the stresses S_{xx}, S_{xz}, S_{zx}, and S_{zz} have the obvious definitions. The equation is expressed in the latter form because the right-hand side of each equation can be expressed in divergence form. Again, since the source terms F_1 and F_2 are usually localized, they are ignored here.

THE 1-D WAVE EQUATION

The technique is derived for the 1-D acoustic and scalar elastic wave equations for several reasons. First, the mathematics is clear and intuitive in one dimension, and the integration extends in a similar manner to the acoustic 2-D equation and also to the vector elastic 2-D equations under minor adjustments. Lin et al. (1990) derive the stability conditions for the 1-D case and show that this scheme gives the analytical solution for any number of interfaces under proper grid refinement at the nodes. Second, these equations can be used to model a horizontal plane wave reflecting off a horizontal plane interface or the motion or pressure disturbance along an interface and are therefore of geophysical importance in their own right. (Figure 8 is an example of this.) It is also well known (Richtmeyer and Morton, 1967) that if the CFL limit is met, the finite-difference solution is equal to the analytic solution at the grid points. Thus the error in the finite-difference solution is due to the conditions' approximation at the interface. Assume that the interface in one dimension occurs at $x = 0$. The 1-D model is illustrated in Figure 1. The acoustic equation system for this 1-D model from equation (1) is

$$p_t + c^2(\rho_0 v)_x = 0,$$
$$v_t + \frac{1}{\rho_0} p_x = 0. \tag{5}$$

The physical conditions at the interface are continuity of the pressure and velocity: $p(0^+, t) = p(0^-, t)$ and $v(0^+, t) = v(0^-, t)$, where

$$(0^{\pm}, t) \equiv \lim_{x \to 0^{\pm}} (x, t).$$

The corresponding equation for u is

$$u_{tt} - c^2 u_{xx} = 0, \tag{6}$$

or

$$\frac{1}{\rho_0 c^2} u_{tt} - \left(\frac{1}{\rho_0} u_x\right)_x = 0, \tag{7}$$

when ρ_0 is piecewise constant. Since $p = -u_t$ and $v = (1/\rho_0)\, u_x$, the continuity conditions at the interface are

$$u_t(0^+, t) = u_t(0^-, t)$$

and

$$\frac{1}{\rho_0^+} u_x(0^+, t) = \frac{1}{\rho_0^-} u_x(0^-, t).$$

In equation (3), the velocity does not occur explicitly for the interface conditions.

The 1-D elastic equation is

$$\rho_0 u_{tt} - \frac{\partial}{\partial x}(\alpha u_x) = 0. \tag{8}$$

The conditions at the interface are

$$u(0^+, t) = u(0^-, t)$$

and

$$\alpha^+ u_x(0^+, t) = \alpha^- u_x(0^-, t).$$

Since we are interested in equations (7) and (8), we consider the variable coefficient equation

$$\alpha(x) u_{tt}(x, t) - [b(x) u_x(x, t)]_x = 0, \tag{9}$$

where $a = 1/\rho_0 c^2$ and $b = 1/\rho_0$ in equation (7) and $a = \rho_0$ and $b = \alpha$ in equation (8). We integrate equation (8) across the interface $x = 0$ to get ($\varepsilon > 0$)

$$\begin{aligned} \int_{-\varepsilon}^{\varepsilon} a u_{tt}\, dx &= \int_{-\varepsilon}^{\varepsilon} (b u_x)_x\, dx \\ &= b u_x \Big|_{-\varepsilon}^{\varepsilon} \\ &= b(\varepsilon) u_x(\varepsilon, t) - b(-\varepsilon) u_x(-\varepsilon, t). \end{aligned} \tag{10}$$

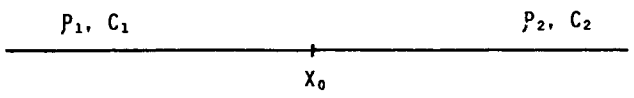

FIG. 1. Two media joined at x_0 to form one model to study interface conditions for 1-D acoustic and elastic-wave propagation occurring in seismic problems.

On substituting appropriate values for a and b,

$$a^- \int_{-\varepsilon}^{0} u_{tt}\, dx + a^+ \int_0^{\varepsilon} u_{tt}\, dx = b^+ u_x(\varepsilon, t) - b^- u_x(-\varepsilon, t). \tag{11}$$

Using the mean value theorem for integrals,

$$[a^- u_{tt}(x_0^-, t) + a^+ u_{tt}(x_0^+, t)]\varepsilon = b^+ u_x(\varepsilon, t) - b^- u_x(-\varepsilon, t), \tag{12}$$

where $-\varepsilon \le x_0^- \le 0$ and $0 \le x_0^+ \le \varepsilon$. On letting ε approach 0, this gives

$$b^+ u_x(0^+, t) = b^- u_x(0^-, t), \tag{13}$$

because, for both the acoustic and elastic 1-D wave equations, u_{tt} is continuous at $x = 0$. Therefore, if equation (9) is used at the grid points away from the interface in the numerical schemes and equation (11) is used at the interface in the numerical schemes, the physical conditions will be accurately calculated if ε (the space grid) is close to 0. Of course, the grid size, which is dependent upon the model being studied, introduces truncation error into the scheme. This derivation is also the method used to obtain the physical conditions needed at an interface. It is presented here because the left-hand side of equation (12) is the expression we are interested in approximating.

The finite-difference approximations for equations (9) and (12) are presented in two steps. The space grids are given by $x_j = j\Delta x$, the time grids by $t^n = n\Delta t$, and $u(j\Delta x, n\Delta t)$ by u_j^n. The finite-difference approximation to equation (9) is then

$$a(u_j^{n+1} - 2u_j^n + u_j^{n-1}) - \gamma b(u_{j+1}^n - 2u_j^n + u_{j-1}^n) = 0,$$

for $j \neq 0$, where centered-difference approximations are used for u_{xx} and u_{tt}, $\gamma = (\Delta t/\Delta x)^2$, $a = a^-$, $b = b^-$ when $j < 0$, and $a = a^+$, $b = b^+$ when $j > 0$. On simplifying,

$$u_j^{n+1} = 2u_j^n - u_j^{n-1} + A(u_{j+1}^n - 2u_j^n + u_{j-1}^n), \tag{14}$$

for $j \neq 0$, where $A = \gamma b/a$. At $x = 0$, we approximate equation (11) by using the mean value theorem for integrals on the left-hand side, let $\varepsilon = \Delta x/2$, and expand $u_{tt}(x_0, t)$ around $x_0 = 0$. On the right-hand side one-sided differences for u_x are used, yielding the second-order accurate approximation

$$\left(\frac{a^+ + a^-}{2\Delta t^2}\right)(u_0^{n+1} - 2u_0^n + u_0^{n-1})\Delta x = \frac{b^+}{\Delta x}(u_1^n - u_0^n) - \frac{b^-}{\Delta x}(u_0^n - u_{-1}^n). \tag{15}$$

Solving for u_0^{n+1} gives

$$u_0^{n+1} = 2u_0^n - u_0^{n-1} + \left(\frac{2\gamma}{a^+ + a^-}\right)[b^+ u_1^n - (b^+ + b^-)u_0^n + b^- u_{-1}^n]. \tag{16}$$

This is the equation used to approximate the solution to equation (9) at the interfaces and is one difference between our method and other techniques. The error is seen to be $O(\Delta x^2)$. Therefore equations (14) and (16) are used to

approximate for the pressures and displacements in one dimension.

Since casting the 1-D scalar wave equation into its corresponding finite-difference equation is similar to deriving the equations governing the motion of masses in a line coupled by springs, the scheme presented above maintains this similarity. If the time derivative in equation (15) were not approximated, the result would be

$$\left(\frac{a^+ + a^-}{2}\right)\Delta x u_0'' = \frac{b^+}{\Delta x}u_1 - \frac{b^+ + b^-}{\Delta x}u_0 + \frac{b^+}{\Delta x}u_{-1}, \qquad (17)$$

where $u_0'' = (\partial^2/\partial t^2)u_0$. This is the differential equation governing the motion of a mass of size $[(a^+ + a^-)/2]\Delta x$ attached to two other masses by springs with spring constants $b^-/\Delta x$ and $b^+/\Delta x$ and is equivalent to equation (15). Also note that if the physical conditions

$$u(0^+, t) = u(0^-, t)$$

and

$$b^+ u_x(0^+, t) = b^- u_x(0^-, t)$$

are used instead of the integral, the equation at the interface in the finite-difference approximations is

$$b^+\left(\frac{u_1 - u_0}{\Delta x}\right) = b^-\left(\frac{u_0 - u_{-1}}{\Delta x}\right) + (b^- + b^+)O(\Delta x) \qquad (18)$$

for all t; or, upon differentiating this equation, we obtain

$$u_0'' = \left(\frac{1}{b^- + b^+}\right)(b^+ u_1'' + b^- u_{-1}'') + O(\Delta x^2). \qquad (19)$$

Using equation (14) to approximate u_1'' and u_{-1}'' gives

$$u_0'' = \left(\frac{1}{b^+ + b^-}\right)\left[\frac{(b^+)^2}{a^+\Delta x^2}(u_2 - 2u_1 + u_0) + \frac{(b^-)^2}{a^-\Delta x^2}(u_0 - 2u_{-1} + u_{-2})\right], \qquad (20)$$

which is a weighted, centered-difference approximation to $u_{tt} = Bu_{xx}$, for appropriate B, and is justified for the above derivation since u_{tt} is continuous at $x = 0$. Therefore, equation (15), derived from integrating across the interface, is similar to equation (20), which explicitly treats the interface condition. Finally, if centered differences are applied directly to equation (9), we obtain

$$(au_{tt})_j = \frac{1}{\Delta x}[(bu_x)_{j+1/2} - (bu_x)_{j-1/2}], \qquad (21)$$

$$a_j u_j'' = b_{j+1/2}\left(\frac{u_{j+1} - u_j}{\Delta x^2}\right) - b_{j-1/2}\left(\frac{u_j - u_{j-1}}{\Delta x^2}\right),$$

and if we set $a_0 = (a^+ + a^-)/2$, $b_{1/2} = b^+$, and $b_{-1/2} = b^-$ and discretize u_j'' in time, equation (16) results. Again, this integral scheme in one dimension agrees with the natural methods for handling the interface conditions.

The main difference between equation (16) and the schemes derived by Kelly et al. (1976) is that more emphasis is placed on the term appearing on the left-hand side. Also, we explicitly account for the boundary conditions and note that errors are introduced in approximating u_x and the integral on the left-hand side. In the 2-D derivation, more consideration is given to the shape of the interface and curved interfaces can be treated more accurately than with standard methods. We now compare our scheme with that given by Kelly et al. (1982) for equation (3) at the interface

$$p_0^{n+1} = 2p_0^n - p_0^{n-1} + \lambda(Ap_1^n - Bp_0^n + Cp_{-1}^n), \qquad (22)$$

where

$$\lambda = \frac{\rho_0^+(c_0^+)^2 + \rho_0^-(c_0^-)^2}{4\Delta x}\Delta t^2,$$

$$A = \frac{\frac{1}{\rho_0^+} + D}{\Delta x},$$

$$B = \frac{\frac{1}{\rho_0^-} + D}{\Delta x},$$

and

$$D = \frac{1}{2}\left(\frac{1}{\rho_0^+} + \frac{1}{\rho_0^-}\right).$$

In Figures 2 and 3, the finite-difference solution for the geometry shown in Figure 1 using equation (22) is compared

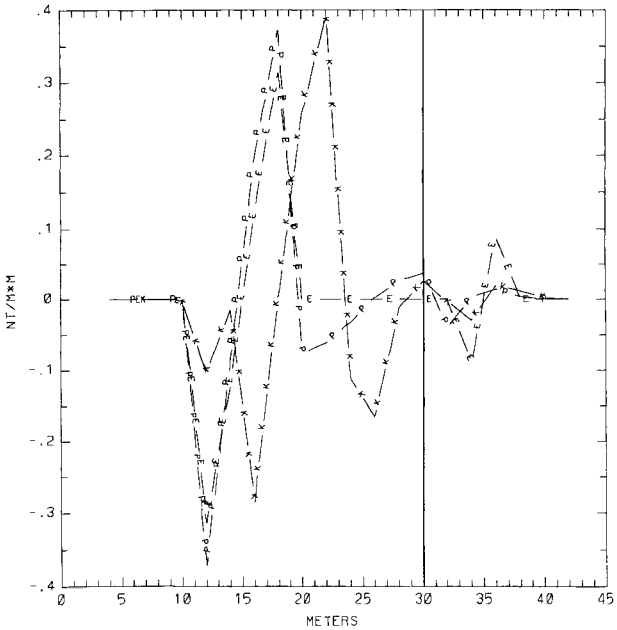

FIG. 2. A snapshot of the pressure distribution at 9.99 ms for the 1-D heterogeneous model of Figure 1. The three graphs are K for the Kelly scheme, P for the scheme presented in the paper, and E for the exact solution. The vertical line at 30 m represents the interface.

with the solution to equation (14) and equation (16) and the exact solution to equation (5). In Figures 2 and 3, $c^- = 6000$ m/s, $c^+ = 2000$ m/s, $\rho^- = 7500$ kg/m^3, $\rho^+ = 2800$ kg/m^3, $\Delta t = 0.33$ ms, $\Delta x = 2.00$ m, and the source is a single period of the sine wave starting to the left of the interface (30.00 m in Figure 2). We specifically chose Δt and Δx so that $c\Delta t/\Delta x = 1$ to ensure that all three solutions would agree and there would be no dispersion until the pulse reaches the interface. Figure 2 shows the pressure distribution at .005 s and Figure 3 represents $p(0, t)$, the pressure at the interface. The discrepancy between the exact solution and the finite-difference solutions can only be worse in 2-D and 3-D wave propagation problems.

THE 2-D ACOUSTIC EQUATION

For the 2-D problem, we assume the well-defined interfaces can be described locally by a function $f(x, z) = 0$ as shown in Figure 4. In the derivation we consider a single interface; in the Appendix, we discuss some interesting approximations for the interfaces.

The necessary equations for the model in Figure 4 are equation (1), with $\mathbf{x} = (x, z)$, and the equations requiring p and $\mathbf{v} \cdot \mathbf{n}$ to be continuous along the interface, where $\mathbf{n}$ is the unit normal to the curve where $f(x, z) = 0$. The equation for u [equation (2)] can be written as

$$\frac{1}{\rho c^2} u_{tt} - \nabla \cdot \left(\frac{1}{\rho_0} \nabla \mathbf{u} \right) = 0,$$

since ρ_0 and c are piecewise constants. The interface conditions are that $p = -u_t$ and $\mathbf{v} \cdot \mathbf{n} = (1/\rho_0)\, \nabla \mathbf{u} \cdot \mathbf{n}$ be continuous along the curve where $f(x, z) = 0$.

To use the principles developed for the 1-D equations, we consider

$$a u_{tt} - \nabla \cdot (b \nabla \mathbf{u}) = 0 \tag{23}$$

for equation (2) with $a = 1/\rho_0 c^2$ and $b = 1/\rho_0$ for the acoustic equation with interfaces. We note that for the appropriate choices of a and b, equation (23) can also be used for the elastic SH equation. The centered-difference approximation for a grid point lying near the interface in Figure 4 is

$$\begin{aligned} u_{jk}^{n+1} = {} & 2u_{jk}^{n} - u_{jk}^{n-1} \\ & + \frac{\Delta t^2}{a_{jk}} \left\{ \frac{1}{\Delta x^2} \left[b_{j+1/2,k} u_{j+1,k}^{n} - (b_{j+1/2,k} \right. \right. \\ & \left. + b_{j-1/2,k}) u_{jk}^{n} + b_{j-1/2,k} u_{j-1,k}^{n} \right] \\ & + \frac{1}{\Delta z^2} \left[b_{j,k+1/2} u_{j,k+1}^{n} - (b_{j,k+1/2} + b_{j,k-1/2}) u_{jk}^{n} \right. \\ & \left. \left. + b_{j,k-1/2} u_{j,k-1}^{n} \right] \right\}, \end{aligned} \tag{24}$$

where $a_{jk} = (\alpha a_1 + \beta a_2)$, $b_{j+1/2,k}$, $b_{j-1/2,k}$, $b_{j,k-1/2}$, $b_{j,k+1/2} = b_1$ or b_2 depending on whether $[(j \pm 1/2)\,\Delta x, \Delta z]$ and $[j\Delta x, (k \pm 1/2)\Delta z]$ are above or below the interface (see Figure 4), and α and β give the percentage of the grid block above and below the interface, respectively, and $u_{jk}^{n} = u(j\Delta x, k\Delta z, n\Delta t)$. This scheme is derived by integrating equation (23) over a grid block containing an interface, using the divergence theorem on the right-hand side and splitting the

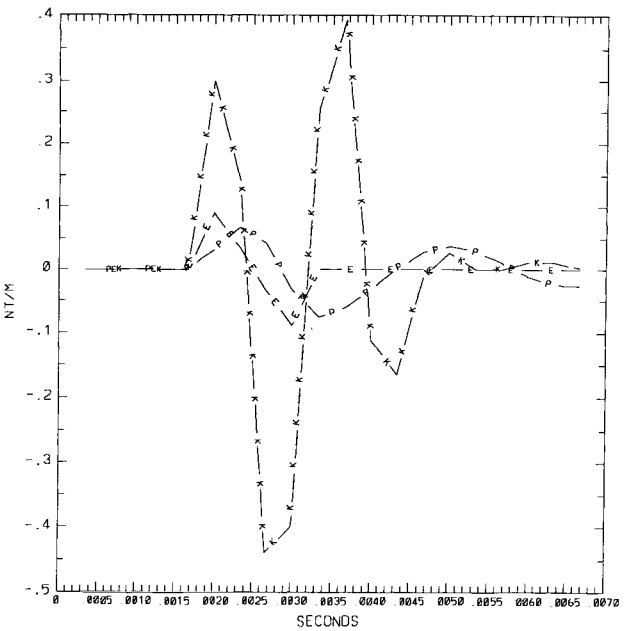

FIG. 3. The motion of the interface grid point of Figure 1 using the three schemes. K is the Kelly scheme, P is the scheme in the paper, and E is the exact solution.

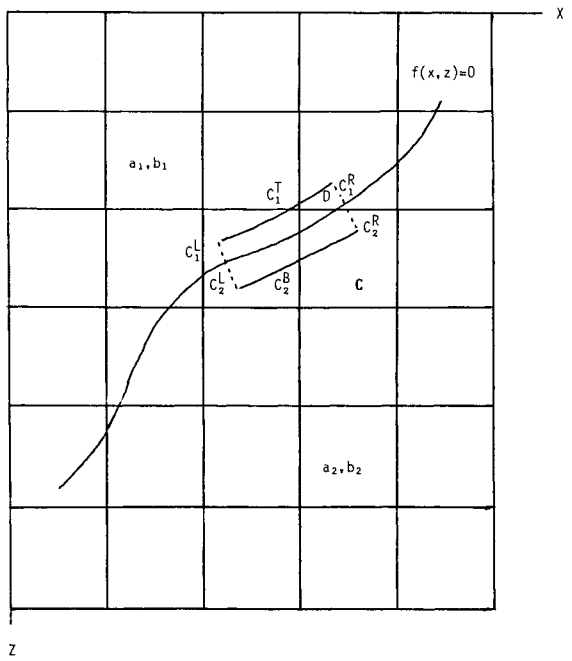

FIG. 4. A cross-section of the earth where two materials are in contact along a curved boundary. The density, sound speed, and Lamé parameters change only at the boundary.

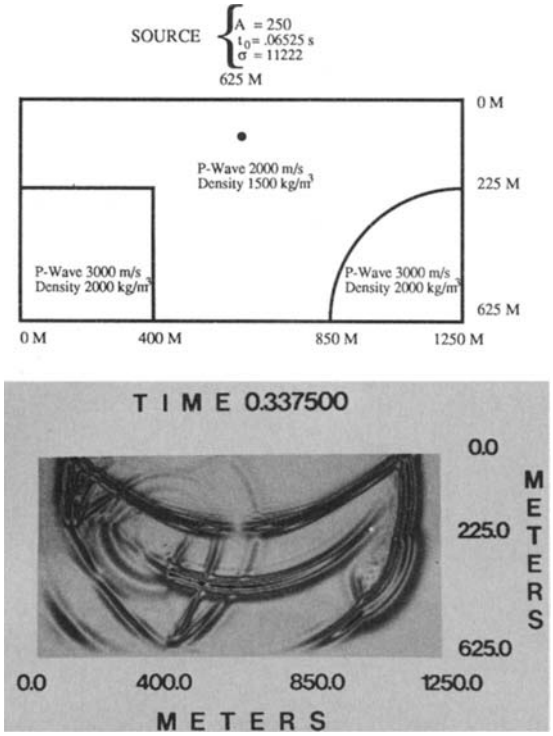

FIG. 5. Acoustic-wave snapshots presenting reflected and transmitted sound waves off a 90-degree corner and a smooth corner for analysis using the finite-difference scheme presented in the paper.

integral on the left-hand side as in the 1-D case. The procedure is carried out in the Appendix. The case where $(j\Delta x, k\Delta z)$ lies on the interface is also treated. Again the node at (j, k) can be considered to be the location of a mass attached to four springs. For the general scheme at a grid point, we let $b_{j+1/2,k} = 1/2(b_{j+1,k+1} + b_{j+1,k-1})$ and $b_{j-1/2,k} = 1/2(b_{j-1,k+1} + b_{j-1,k-1})$. This can be obtained easily by applying the integration scheme presented in the Appendix to general interfaces. For the pressure distribution $p^n_{jk} = p(j\Delta x, k\Delta z, n\Delta t)$, set $p^n_{jk} = (u^n_{jk} - u^{n+1}_{jk})/\Delta t$, or use $p^n_{jk} = (u^{n-1}_{jk} - u^{n+1}_{jk})/2\Delta t$ for better accuracy.

We now show that the correct physical limits are met by the appropriate physical variables. We integrate equation (23) over the domain D in Figure 4. C is the curved boundary of D, C_1^T and C_2^B are the parts of C parallel to $f(x, z) = 0$, and C_i^L and C_i^R $(i = 1, 2)$ are of length ε. Integrating and breaking up the integrals over each piece formed by D and C and using the divergence theorem gives

$$\int_D au_{tt}\, dA = \int_D \nabla \cdot (b\nabla \mathbf{u})\, dA,$$

$$\int_{D_1} au_{tt}\, dA + \int_{D_2} au_{tt}\, dA = \oint_C b\nabla \mathbf{u} \cdot \mathbf{n}\, dA, \tag{25}$$

$$a_1 \int_{D_1} u_{tt}\, dA + a_2 \int_{D_2} u_{tt}\, dA = \oint_{C_2} b_2 \nabla \mathbf{u} \cdot \mathbf{n}_2\, ds + \oint_{C_1} b_1 \nabla \mathbf{u} \cdot \mathbf{n}_1\, dS,$$

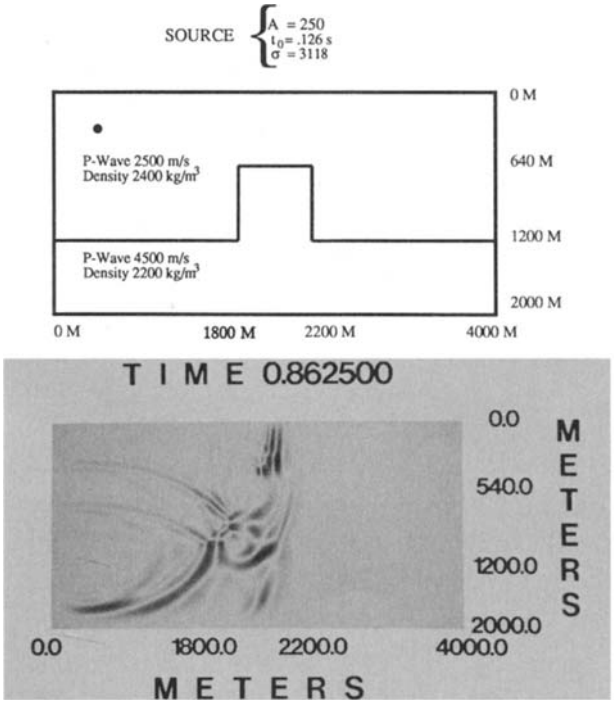

FIG. 6. Acoustic-wave snapshots presenting reflected and transmitted waves off a salt dome for analyzing corner waves using the finite-difference scheme presented in the paper.

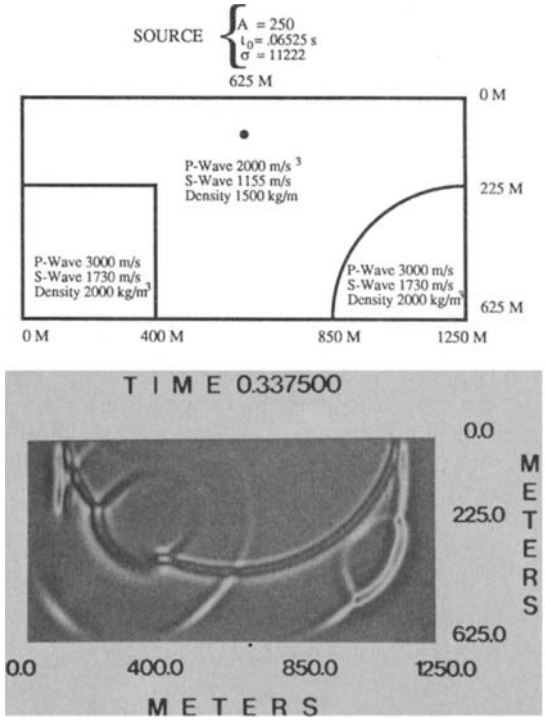

FIG. 7. The elastic-wave snapshots of the model in Figure 5.

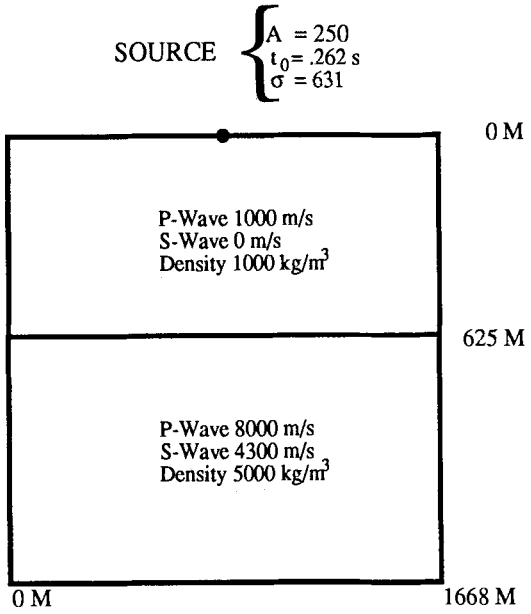

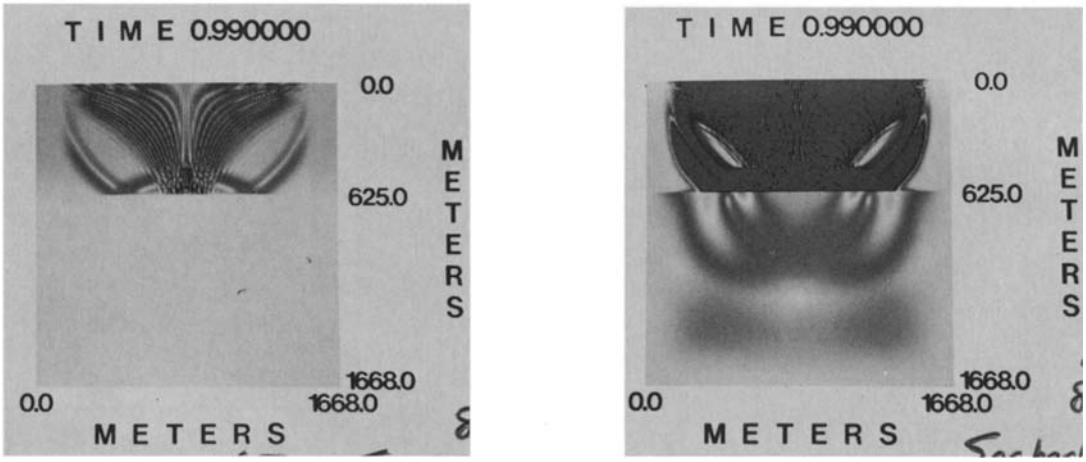

FIG. 8. Snapshots of a fluid over a basalt region using the scheme for the elastic-wave equation. The image on the right has been intensified to highlight the wave transmitted through the basalt region.

where $\mathbf{n}$, $\mathbf{n}_1$, and $\mathbf{n}_2$ are the normals to C, C_1, and C_2, respectively. Approximating the integrals on the left-hand side using the mean value theorem for integrals and performing the integrals on the right-hand side over each part composing C_1 and C_2 gives

$$a_1 u_{tt}(x_1, z_1, t)\Delta D_1 + a_2 u_{tt}(x_2, z_2, t)\Delta D_2$$

$$= \oint_{C_2^B} b_2 \nabla \mathbf{u} \cdot \frac{\nabla f}{\|\nabla f\|}\, dS + \oint_{C_2^L} b_2 \nabla \mathbf{u} \cdot \mathbf{n}_2^L\, ds$$

$$+ \oint_{C_2^R} b_2 \nabla \mathbf{u} \cdot \mathbf{n}_2^R\, ds + \oint_{C_1^L} b_1 \nabla \mathbf{u} \cdot \mathbf{n}_1^L\, ds$$

$$+ \oint_{C_1^T} b_1 \nabla \mathbf{u} \cdot \left(-\frac{\nabla f}{\|\nabla f\|}\right) ds + \oint_{C_1^R} b_1 \nabla \mathbf{u} \cdot \mathbf{n}_1^R\, ds$$

$$= \oint_{C_2^B} b_2 \nabla \mathbf{u} \cdot \frac{\nabla f}{\|\nabla f\|}\, ds + \int_{C_1^T} b_1 \nabla \mathbf{u} \cdot \left(-\frac{\nabla f}{\|\nabla f\|}\right) ds$$

$$+ b_2 \nabla \mathbf{u} \cdot \mathbf{n}_2^L \Big|_{P_2^L} \varepsilon + b_2 \nabla \mathbf{u} \cdot \mathbf{n}_2^R \Big|_{P_2^R} \varepsilon + b_1 \nabla \mathbf{u} \cdot \mathbf{n}_1^R \Big|_{P_1^R} \varepsilon$$

$$+ b_1 \nabla \mathbf{u} \cdot \mathbf{n}_1^L \Big|_{P_1^L} \varepsilon,$$

where (x_i, z_i) is in D_i, n_i^M and P_i^M, for $M = L, R$ and $i = 1, 2$ are the normals to the curves and points on the curves,

respectively, in Figure 4. Letting ε approach 0 and using the continuity of u_{tt} on the interface ($p = -u_t$) gives

$$0 = \oint_C \left[b_2 \nabla \mathbf{u} \cdot \frac{\nabla f}{\|\nabla f\|} - b_1 \nabla \mathbf{u} \cdot \frac{\nabla f}{\|\nabla f\|} \right] dS,$$

where C is the section of the curve where $f(x, z) = 0$ parallel to C_1^T and C_2^B. Since the length of C is arbitrary, this gives

$$b_2 \nabla \mathbf{u} \cdot \mathbf{n} = b_1 \nabla \mathbf{u} \cdot \mathbf{n}$$

along $f(x, z) = 0$; that is, $b\nabla \mathbf{u} \cdot \mathbf{n}$ is continuous along the interface. Since $\mathbf{v} = b\nabla \mathbf{u}$, this gives the physical requirement. Therefore, if the grids are determined by being parallel to the curve where $f(x, z) = 0$, using equation (24) to approximate u_{jk}^n for all grid points on the interface gives an approximation that agrees with the actual value with error the order of the grid size.

This is the derivation used to obtain the physical conditions at an interface from the equations. Also, note that the divergence form of equation (23) gives a natural scheme at an interface. Since, equation (23) has the same form in three dimensions, to obtain the scheme for the 3-D acoustic equations, we apply the same technique and use the divergence theorem for three dimensions with approximate surface and volume integrals instead of line and surface integrals.

Hence grid points on or near an interface should be assigned a value by using a centered difference for u_{tt} on the left-hand side of equation (24) and using a numerical scheme to approximate the integrals on the right-hand side. We emphasize that even if the stability requirement (Richtmeyer and Morton, 1967) for equation (23) is kept for grid points away from the interface, instabilities and dispersion can still be caused by the interface (Sochacki, 1985; Trefethen, 1985). However, as the figures indicate, stability is maintained with this scheme if the von Neumann stability criterion [$v\Delta t/\Delta x \leq 1/\sqrt{2}$ (for $\Delta x = \Delta z$), where v is the maximum sound speed in the heterogeneous model] is kept. A more detailed stability analysis for two dimensions will be presented later and is similar to the analysis in Lin et al.

Although the above derivation is for piecewise constants a and b, the scheme can be used for variables a and b. For example, if ρ_0 and c vary over a grid block in Figure 4, we have to use equation (2); and to accomplish this in equation (23), we let $a = 1/c^2$ and $b = 1$. In equation (25), the left-hand side integral would not be broken up and the approximation

$$\int_D a u_{tt}\, dA = u_{tt}(x_0, z_0, t) \int_D a\, dA$$

could be used. We would then calculate the integral on the right-hand side. Here (x_0, z_0) would be the grid point at which u is to be determined.

Snapshots

Figure 5 and Figure 6 represent pressure distributions for heterogeneous media using the technique presented here at the interface. The model in Figure 5 takes the corner problem from the pioneering paper of Kelly et al. (1976). Our model adds a smooth circular region in the right bottom corner with the same parameters. The smooth corner has been inserted to show that our scheme can handle both straight and curved interfaces accurately. The model in Figure 6 represents a squared salt dome and is similar to the model presented in Virieux (1984). In both models, the source in time is the derivative of the Gaussian with the form

$$f(t) = A(t - t_0) \exp\left[-\sigma(t - t_0)^2\right] \tag{26}$$

and the absorbing boundary conditions used are those presented in Sochacki et al. (1987). Our source configurations were chosen for each snapshot so that the dispersion would be minimized and an approximate 20 Hz source would result.

The model for Figure 5 has a horizontal extent of 1250 m and a vertical extent of 625 m. The upper region has a density of 1500 kg/m^3 and a sound speed of 2000 m/s, while the lower corners have a density of 2000 kg/m^3 and a sound speed of 3000 m/s. The grid size for the scheme is 4.17 m and the time step is 0.0009 s. The source is located at (625, 125.5)

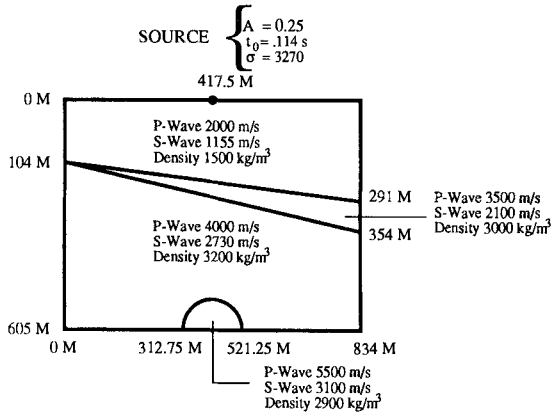

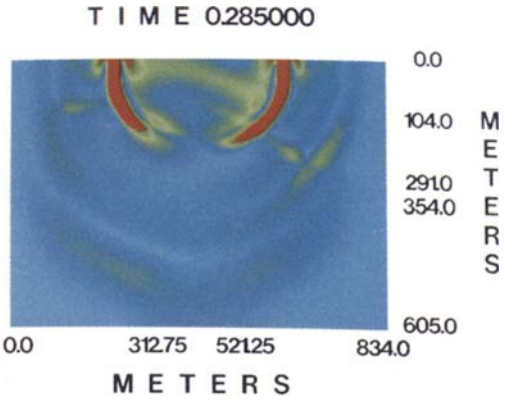

FIG. 9. Elastic-wave amplitude snapshots for a complicated region containing a wedge and a dome of varying velocities and densities.

and has parameters $A = 250$, $t_0 = 0.06525$ s, and $\sigma = 11222$ and acts for 0.1305 s in equation (26).

In Figure 5, note the difference in the reflected, transmitted, and diffracted waves from the two corners. The left corner causes characteristic changes in the wave forms as seen in Kelly et al. (1976), while the right corner allows smoother changes in the waveforms, as expected. In both cases, the shape of the interface is recognizable.

The model for Figure 6 has a horizontal extent of 4000 m and a vertical extent of 2000 m. The upper region has a density of 1750 kg/m^3 and a sound speed of 2500 m/s, while the dome has a density of 2337 kg/m^3 and a sound speed of 4500 m/s according to the model in Virieux (1984). The grid size is 10 m and the time step is 0.0015 s. The source is located at (420, 210) and has parameters $A = 250$, $t_0 = .126$ s, and $\sigma = 3118$ and acts for .252 s in equation (26).

The source in the model is offset to show the differences in wave motion at the corners. We note the corner waves and head waves are similar to those described in Virieux (1984). The difference in waves traveling from the low-velocity region into the dome and from the dome to the low-velocity region is easily seen and is physically reasonable.

THE 2-D ELASTIC WAVE EQUATION

The physical requirement at an interface for elastic *P-SV* wave propagation is that $(S_{xx}, S_{xz}) \cdot n$ and $(S_{zx}, S_{zz}) \cdot n$ must be continuous (Boresi and Lynn, 1974). For horizontal and vertical interfaces, these conditions can be handled with finite-difference schemes similar to those presented by Vidale and Clayton (1986) and Sochacki et al. (1987) for free surfaces. However, for slanted and curved interfaces, these schemes are much more difficult to employ. In the following, we briefly show that the integration scheme presented above can also be used at the interfaces for equation (4a). (Again, we ignore the source terms.)

The technique is applied to each component of the elastic wave equation. To apply the scheme above, we write equation (4a) in divergence form as

$$\rho_0 u_{tt} = \nabla \cdot (S_{xx}, S_{xz}),$$
$$\rho_0 w_{tt} = \nabla \cdot (S_{zx}, S_{zz}), \tag{27}$$

and again integrate using the divergence theorem. The mixed derivatives complicate the integration and more care has to be used in integrating the S_{xz} and S_{zx} terms. The scheme obtained is

$$\begin{aligned}
u''_{jk} = \frac{1}{\bar{\rho}}\Bigg[& \frac{(\lambda+2\mu)_{j+1k+1} + (\lambda+2\mu)_{j+1k-1}}{2} \frac{u_{j+1k} - u_{jk}}{\Delta x^2} \\
& - \frac{(\lambda+2\mu)_{j-1k+1} + (\lambda+2\mu)_{j-1k-1}}{2} \frac{u_{jk} - u_{j-1k}}{\Delta x^2} \\
& + \frac{\mu_{j+1k+1} + \mu_{j-1k+1}}{2} \frac{u_{j+1k} - u_{jk}}{\Delta z^2} \\
& - \frac{\mu_{j+1k-1} + \mu_{j-1k-1}}{2} \frac{u_{jk} - u_{jk-1}}{\Delta z^2} \\
& + \lambda_{j+1k+1} \frac{w_{j+1/2k+1} - w_{j+1/2k}}{2\Delta x \Delta z} \\
& + \mu_{j+1k+1} \frac{w_{j+1k+1/2} - w_{jk+1/2}}{2\Delta x \Delta z} \\
& + \mu_{j-1k+1} \frac{w_{jk+1/2} - w_{j-1k+1/2}}{2\Delta x \Delta z} \\
& - \lambda_{j-1k+1} \frac{w_{j-1/2k+1} - w_{j-1/2k}}{2\Delta x \Delta z} \\
& - \lambda_{j-1k-1} \frac{w_{j-1/2k} - w_{j-1/2k-1}}{2\Delta x \Delta z} \\
& - \mu_{j-1k-1} \frac{w_{jk-1/2} - w_{j-1k-1/2}}{2\Delta x \Delta z} \\
& - \mu_{j+1k-1} \frac{w_{j+1k-1/2} - w_{jk-1/2}}{2\Delta x \Delta z} \\
& + \lambda_{j-1k-1} \frac{w_{j+1/2k} - w_{j+1/2k-1}}{2\Delta x \Delta z} \Bigg] \\
= R^u_{jk};
\end{aligned}$$

$$\begin{aligned}
w''_{jk} = \frac{1}{\bar{\rho}}\Bigg[& \frac{(\lambda+2\mu)_{j+1k+1} + (\lambda+2\mu)_{j-1k+1}}{2} \frac{w_{jk+1} - w_{jk}}{\Delta z^2} \\
& - \frac{(\lambda+2\mu)_{j+1k-1} + (\lambda+2\mu)_{j-1k-1}}{2} \frac{w_{jk} - w_{jk-1}}{\Delta z^2} \\
& + \frac{\mu_{j+1k+1} + \mu_{j+1k-1}}{2} \frac{w_{j+1k} - w_{jk}}{\Delta x^2} \\
& - \frac{\mu_{j-1k+1} + \mu_{j-1k-1}}{2} \frac{w_{jk} - w_{j-1k}}{\Delta x^2} \\
& + \mu_{j+1k+1} \frac{u_{j+1/2k+1} - u_{j+1/2k}}{2\Delta x \Delta z} \\
& + \lambda_{j+1k+1} \frac{u_{j+1k+1/2} - u_{jk+1/2}}{2\Delta x \Delta z} \\
& + \lambda_{j-1k+1} \frac{u_{jk+1/2} - u_{j-1k+1/2}}{2\Delta x \Delta z} \\
& - \mu_{j-1k+1} \frac{u_{j-1/2k+1} - u_{j-1/2k}}{2\Delta x \Delta z} \\
& - \mu_{j-1k-1} \frac{u_{j-1/2k} - u_{j-1/2k-1}}{2\Delta x \Delta z} \\
& - \lambda_{j-1k-1} \frac{u_{jk-1/2} - u_{j-1k-1/2}}{2\Delta x \Delta z}
\end{aligned}$$

$$- \lambda_{j+1k-1} \frac{u_{j+1k-1/2} - u_{jk-1/2}}{2\Delta x \Delta z} + \mu_{j-1k-1} \frac{u_{j+1/2k} - u_{j+1/2k-1}}{2\Delta x \Delta z} \Bigg] = R^w_{jk}, \quad (28)$$

where $\bar{\rho}$ is the average of ρ_0 at the grid point $(j\Delta x, k\Delta z)$. On replacing the time derivatives by centered differences, we obtain the scheme

$$u^{n+1}_{jk} = 2u^n_{jk} - u^{n-1}_{jk} + \Delta t^2 R^u_{jk},$$
$$w^{n+1}_{jk} = 2w^n_{jk} - w^{n-1}_{jk} + \Delta t^2 R^w_{jk}. \quad (29)$$

The difference between the scheme presented by Kelly et al. (1976) and the one presented here is that the u and w terms involving subscripts $j - 1/2, j + 1/2, k - 1/2$, and $k + 1/2$ have to be approximated. We approximate these terms by the normal method; that is, $u_{j-1/2,k} = 1/2(u_{jk} + u_{j-1,k})$, etc., in order to maintain second-order accuracy. The resulting equations are easily seen to be different from those in Kelly et al. (1976). After making these substitutions, it is straightforward to show that, for λ and μ constant, equation (29) reduces to the standard centered-difference approximation. In the Appendix, we carry out the integration for the u component for a simple example. The integration is similar for more complicated interfaces, and in all cases equation (29) can be used. The figures again indicate that stability is maintained in the elastic case if the von Neumann stability criterion $(\alpha^2 + \beta^2)^{1/2}\Delta t/\Delta x \leq 1$ (for $\Delta x = \Delta z$, see Alterman and Lowenthal, 1970), where α is the largest P-wave velocity and B is the corresponding S-wave velocity of the heterogeneous model, is maintained.

To show that the interface conditions are approximately satisfied, we integrate over D in equation (4a). Using the mean value theorem on the right-hand side and the divergence theorem on the left-hand side of the equation for u, and letting ε approach 0 gives

$$\oint_C \left[(S^2_{xx}, S^2_{xz}) \cdot \frac{\nabla f}{\|\nabla f\|} - (S^1_{xx}, S^1_{xz}) \cdot \frac{\nabla f}{\|\nabla f\|} \right] ds = 0.$$

Again, it is seen that if the grids are parallel to the interface, approximating the area integrals used in equation (4a) gives an accurate estimate of the physical conditions for elastic motion at an interface. Therefore, for rectangular grids, it is recommended that approximations to the area integrals applied to equation (4a) be used for approximations to u^n_{jk} and w^n_{jk} for grid points on or near an interface. The extension to the variable-coefficient case is as outlined in the acoustic case. The extension to the full 3-D vector elastic equations is done similarly by performing the acoustic 3-D method to each of the three components of these equations.

Snapshots

The next three figures represent the amplitude of elastic waves propagating in various heterogeneous media. Figure 7 is the same model as in Figure 5 with an S-wave velocity of 1155 m/s in the top region and 1730 m/s in the lower corners. Figure 8 represents the motion generated by a source in a fluid over a basalt region and shows that the scheme can handle large parameter contrasts. Figure 9 depicts the snapshots for a complicated region of varying velocities and densities. The sources are again the derivative of the Gaussian given in equation (26). The surface sources, surface conditions, and boundary conditions, together with the addition of the curved boundary method in this paper, are handled by the schemes presented in Sochacki et al. (1987).

The snapshots in Figure 7 can be compared with those in Figure 5 and those in Kelly et al. (1976). We note the similarity of the P-waves to the acoustic wave model. The physically reasonable difference in the reflected, transmitted, and diffracted shear waves at the two interfaces is again noted.

The model for Figure 8 has horizontal and vertical extent of 1668 m. The grid size is 8.34 m, the time step is 0.0009 s, the source is located on the surface at 834 m, and has parameters $A = 0.25$, $t_0 = 0.262$ s and $\sigma = 631$, and acts for 0.524 s in equation (26). The top region represents a perfect fluid (zero shear) with P-wave velocity 1000 m/s, density 1000 kg/m^3. The lower basalt region has a P-wave velocity of 8000 m/s, shear-wave velocity of 4300 m/s, and density 5000 kg/m^3. We note the difference in amplitude of the reflected and transmitted waves and the wave motion along the interface. Note the head wave.

The model for Figure 9 illustrates a more realistic geologic formation; it is composed of four layered regions with a salt dome at the bottom and has a horizontal extent of 834 m and a vertical extent of 601 m. The P-wave velocities from top to bottom are 2000 m/s, 3500 m/s, 4000 m/s, and 5500 m/s. The corresponding shear velocities are 1155 m/s, 2100 m/s, 2730 m/s, and 3100 m/s. The grid size is 4.17 m and the time step is 0.0006 s. The source is located on the surface at 417 m and has parameters $A = 0.25$, $t_0 = 0.114$, and $\sigma = 3270$ and acts for 0.228 s in equation (26). We note that the wedge propagates a waveguide effect.

CONCLUSIONS

A technique that can handle curved regular or irregular interfaces has been derived for finite-difference schemes but can be used with other numerical schemes such as the finite element. The scheme can be easily implemented in second-order acoustic and elastic finite-difference solvers, and the same principles can be used in the development of 3-D models. Since the acoustic and elastic-wave equations have been left second order in time for the scheme presented, the pressure and displacements are approximated directly and there is no increase in memory to solve these equations as there is with techniques that treat a system of first-order equations (e.g., see Virieux, 1984, 1986).

Error estimates have been given for the 1-D case and can be obtained for specific models as outlined in the examples of the Appendix. Interface conditions are more accurately treated when the grids are parallel to the interface since the interface conditions depend upon the normal to the interface. By appropriate weighting, the grid orientation problems can be minimized. The form in which the acoustic and elastic-wave equations have been presented has the correct boundary conditions at curved interfaces.

The scheme has been tested on various geometries and can be compared to existing codes. The scheme is stable for both 2-D acoustic and elastic-wave propagation with normal stability. The scheme is also stable in a preliminary 3-D model.

ACKNOWLEDGMENTS

The authors wish to thank an associate editor and reviewers for helpful comments which improved the paper and Patrick O'Leary and Mark Oliver for their help with the graphics. This research was partially supported by NSF grant no. DMS-8712021, ONR contract no. 0014-88-K-0370, and the Institute for Scientific Computation through NSF grant no. RII-8610680.

REFERENCES

Alterman, Z. S., and Loewenthal, D., 1970, Seismic waves in a quarter and three quarter plane: Geophys. J. Roy. Astr. Soc., **20,** 101–126.

Boore, D. M., 1972, Finite-difference methods for seismic wave propagation in heterogeneous materials, *in* Bolt, B. A., Ed., Methods in computational physics, II: Academic Press, Inc.

Boresi, A. P., and Lynn, P. P., 1974, Elasticity in engineering mechanics: Prentice-Hall.

Brown, D. L., 1984, A note on the numerical solution of the wave equation with piecewise continuous smooth coefficients: Math of Comp., **42,** 369–391.

Dougherty, M. E., and Stephen, R. A., 1988, Seismic energy partitioning and scattering in laterally homogeneous ocean crust: Pure and Appl. Geophys., **128,** 195–229.

Ewing, W. M., Jardetzky, W. S., and Press, F., 1957, Elastic waves in layered media: McGraw-Hill Book Co.

Kelly, K. R., Ward, R. W., Treitel, S., and Alford, R. M., 1976, Synethetic seismograms: A finite-difference approach: Geophysics, **41,** 2–27.

Kelly, K. R., Ward, R. W., Treitel, S., and Alford, R. M., 1982, Modeling—The forward method, *in* Jain, K. C., and de Figueiredo, R. J. P., Eds., Concepts and techniques in oil and gas exploration: Soc. Expl. Geophys.

Kummer, B., and Behle, A., 1982, Second-order finite-difference modeling of SH-wave propagation in laterally inhomogeneous media: Bull. Seis. Am., **72,** 793–808.

Landau, L. D., and Lifshitz, M. E., 1959, Fluid mechanics: Pergamon Press.

Levander, A. R., 1988, Fourth-order finite-difference *P-SV* seismograms: Geophysics, **53,** 1425–1436.

Lin, T., Sochacki, J., Ewing, R., and George, J., 1990, Some grid refinement schemes for hyperbolic equations with piece-wise constant coefficients: Math. of Comp., in press.

Madariaga, R., 1976, Dynamics of an expanding circular fault: Bull. Seis. Am., **66,** 639–666.

Mitchell, A. R., 1969, Computational methods in partial differential equations: John Wiley and Sons.

Richtmeyer, R. D., and Morton, K. W., 1967, Difference methods for initial value problems: Interscience Publ.

Sochacki, J., 1985, An analysis of the continuous and finite-difference equations for acoustic and elastic wave phenomena: Ph.D. thesis, Univ. of Wyoming.

Sochacki, J., Kubicheck, R., George, J., Fletcher, W. R., and Smithson, S., 1987, Absorbing boundary conditions and surface waves: Geophysics, **52,** 60–71.

Trefethen, L. N., 1982, Group velocity in finite difference schemes, SIAM Rev., **24,** 113–136.

———, 1985, Stability of finite-difference models containing two boundaries or interfaces: Math of Comp., **45,** 279–300.

Vidale, J. E., and Clayton, R. W., 1986, A stable free-surface boundary condition for two-dimensional elastic finite-difference wave simulation: Geophysics, **51,** 2247–2249.

Virieux, J., 1984, *SH*-wave propagation in heterogeneous media: Velocity-stress finite-difference method: Geophysics, **49,** 1933–1957.

———, 1986, *P-SV* wave propagation in heterogeneous media: Velocity-stress finite-difference method: Geophysics, **51,** 889–901.

APPENDIX

FINITE-DIFFERENCE APPROXIMATIONS NEAR INTERFACES

The Acoustic Case

We consider Figure A-1 and determine approximations at the points P_0, P_1, and P_2 for equation (18) with the interface conditions. This is done using equation (20) in detail for P_0 and then giving the results when applied to P_1 and P_2.

Integrating over the domain D_0 gives

$$\int_{D_0} a u_{tt} = \int_{D_0} \nabla \cdot (b \nabla u). \tag{A-1}$$

Performing the integration on the right-hand side first gives

$$\begin{aligned}\int_{D_0} \nabla \cdot (b\nabla \mathbf{u}) &= \oint_{C_0} b\nabla \mathbf{u} \cdot \mathbf{n} \\ &= \oint_{C_0^1} (b\nabla \mathbf{u}) \cdot \mathbf{n}_0^- \\ &\quad + \oint_{f(x,z)=0} b\nabla \mathbf{u} \cdot \frac{\nabla f}{\|\nabla f\|} + \oint_{C_0^2} b\nabla \mathbf{u} \cdot \mathbf{n}_0^+ \\ &\quad + \oint_{f(x,z)=0} b\nabla \mathbf{u} \cdot \left(-\frac{\nabla f}{\|\nabla f\|}\right) \\ &= \oint_{C_0^1} b\nabla \mathbf{u} \cdot \mathbf{n}_0^- + \oint_{C_0^2} b\nabla \mathbf{u} \cdot \mathbf{n}_0^+,\end{aligned}$$

since $b\nabla \mathbf{u} \cdot \mathbf{n}$ is continuous along the interface. Splitting the integral on the right-hand side gives

$$\begin{aligned}&\oint_{C_0^1} b\nabla \mathbf{u} \cdot \mathbf{n}_0^- + \oint_{C_0^2} b\nabla \mathbf{u} \cdot \mathbf{n}_0^+ \\ &= \int_{P_N}^{P_0^-} b_1 \nabla \mathbf{u} \cdot (-1, 0) + \int_{P_0^-}^{P_R} b_1 \nabla \mathbf{u} \cdot (0, -1) \\ &\quad + \int_{P_R}^{P_0'} b_2 \nabla \mathbf{u} \cdot (0, -1) + \int_{P_0'}^{P_0^+} b_2 \nabla \mathbf{u} \cdot (1, 0) \\ &\quad + \int_{P_0^+}^{P_0''} b_2 \nabla \mathbf{u} \cdot (0, 1) + \int_{P_0''}^{P_N} b_2 \nabla \mathbf{u} \cdot (-1, 0) \\ &= \int_{z_N}^{z_0^-} -b_1 u_x(-dz)\Big|_{x=x_0^-} + \int_{x_0^-}^{x_R} -b_1 u_z\, dx\Big|_{z=0^-}\end{aligned}$$

$$+\int_{x_R}^{x_0^+} -b_2 u_z\,dx\Big|_{z=z_0^-} + \int_{z_0^-}^{z_0^+} b_2 u_x\,dz\Big|_{x=x_0^+}$$

$$+\int_{x_0^+}^{x_0^-} b_2 u_z(-dx)\Big|_{z=z_0^+} + \int_{z_0^+}^{z_N} -b_2 u_x(-dz)\Big|_{x=x_0^-}$$

$$= -b_1 u_x(x_0^-, z_1)(z_N - z_0^-) - b_1 u_z(x_1, z_0^-)$$
$$\times (x_R - x_0^-) - b_2 u_z(x_2, z_0^-)(x_0^+ - x^R)$$
$$+ b_2 u_x(x_0^+, z_2)(z_0^+ - z_0^-) + b_2 u_z(x_3, z_0^+)(x_0^+ - x_0^-)$$
$$- b_2 u_x(x_0^-, z_3)(z_0^+ - z_N),$$

where we have used the mean value theorem for integrals and $y_0^{\pm} = y_0 \pm \Delta x/2$, ($y = x$ or z); $P_L = (x_L, z_L)$, $L = R, N$, $P_0^{\pm} = (x_0^{\pm}, z_0^{\pm})$, $P_0' = (x_0^+, z_0^-)$ and $P_0'' = (x_0^-, z_0^+)$.

Dropping the small grid length terms (see Figure A-1), using centered differences, and replacing z_N with z_0^+, x_R with x_0^+, z_1, z_2 and z_3 with z_0, and x_1 and x_3 with x_0 gives for the right-hand side of equation (A-1)

$$\int_{D_0} \nabla \cdot b(\nabla \mathbf{u}) \approx -b_1\left(\frac{u_{jk} - u_{j-1,k}}{\Delta x}\right)\Delta z + b_2\left(\frac{u_{j+1,k} - u_{jk}}{\Delta x}\right)\Delta z \qquad \text{(A-2)}$$

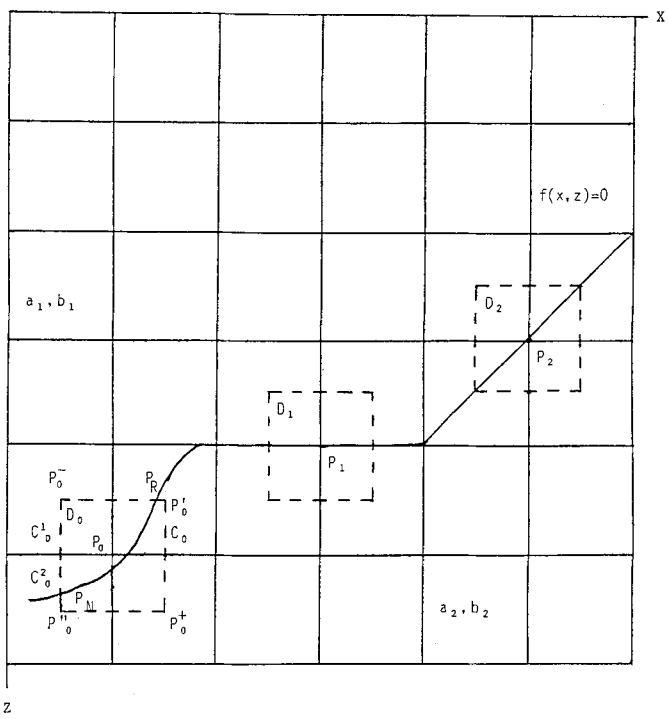

FIG. A-1. A detailed cross-section of the earth similar to Figure 4 for the analysis in the Appendix.

$$-b_1\left(\frac{u_{jk} - u_{j,k-1}}{\Delta z}\right)\Delta x + b_2\left(\frac{u_{j,k+1} - u_{jk}}{\Delta z}\right)\Delta x.$$

Splitting the integral on the left-hand side of equation (A-1) gives

$$\int_{D_0} a u_{tt} = \int_{D_0^2} a_2 u_{tt} + \int_{D_0^1} a_1 u_{tt}$$
$$= a_2 u_{tt}(x_2, z_2, t)\Delta D_0^2 + a_1 u_{tt}(x_1, z_1, t)\Delta D_0^1$$
$$= a_2[u_{tt}(x_0, z_0, t) + O(\Delta x \Delta z)]\Delta D_0^2$$
$$+ a_1[u_{tt}(x_0, z_0, t) + O(\Delta x \Delta z)]\Delta D_0^1$$
$$= (\alpha a_2 + \beta a_1)u_{tt}(x_0, z_0, t) + O(\Delta x \Delta z)$$
$$= A u_{tt}(x_0, z_0, t)\Delta x \Delta z, \qquad \text{(A-3)}$$

where we have used the mean value theorem for integrals and $\alpha = \Delta D_0^2$ and $\beta = \Delta D_0^1$ and equal the area of D_0^2 and D_0^1. Equating (A-2) and (A-3) gives

$$A u_{tt} = \frac{1}{\Delta x^2}[b_2 u_{j+1,k} - (b_1 + b_2)u_{jk} + b_1 u_{j-1,k}]$$
$$+ \frac{1}{\Delta z^2}[b_2 u_{j,k+1} - (b_1 + b_2)u_{jk} + b_1 u_{j,k-1}] \qquad \text{(A-4)}$$

which is equation (19) on replacing u_{tt} by its centered-difference approximation. The error introduced is $O(\Delta x, \Delta z)$ from equation (A-3) and $O(\Delta x^2, \Delta z^2)$ from equation (A-2).

For the horizontal interface at P_1, the finite-difference equation that results on performing the above on equation (A-1) with D_0 replaced by D_1 gives

$$\left(\frac{a_1 + a_2}{2}\right)u_{tt}(x_1, z_1, t)$$
$$= \frac{1}{\Delta x^2}\left[\left(\frac{b_1 + b_2}{2}\right)u_{j+1,k} - (b_1 - b_2)u_{jk} + \left(\frac{b_1 + b_2}{2}\right)u_{j-1,k}\right]$$
$$+ \frac{1}{\Delta z^2}[b_2 u_{j,k+1} - (b_1 + b_2)u_{jk} + b_1 u_{j,k-1}], \qquad \text{(A-5)}$$

which slightly differs from equation (19), unless $b_{j+1/2k} = (b_1 + b_2)/2 = b_{j-1/2k}$. This agrees with the spring-mass model and should be accurate since the grid is parallel to the interface.

For the diagonal interface at P_2, the finite-difference equation is the same as equation (A-4), with $A = (a_1 + a_2)/2$. However, for this case, no small terms have to be dropped.

The derivations presented here can be applied to each equation in equation (7a), leading to equation (21) for Figure 4.

The elastic case

Here, we consider the u component of equation (21) as the point P_1 in Figure A-1. This is done to minimize the notation, but it is straightforward to extend the ideas to points P_0 and P_2. We denote P_1 in this section by $P_1 = (j\Delta x, k\Delta z) = (x_0, z_0)$ and the boundary of D_1 including the interface by C_1. Integrating the u component of equation (21) over D_1 and following the same procedure used in the acoustic case, we obtain

$$\int_{D_1} \rho_0 u_{tt} = \int_{D_1} \nabla \cdot (S_{xx}, S_{xz})$$

$$= \oint_{C_1} (S_{xx}, S_{xz}) \cdot \mathbf{n} = \oint_{C_1} \bar{\mathbf{S}} \cdot \mathbf{n}.$$

We approximate the left-hand side by

$$\int_{D_1} \rho_0 u_{tt} \approx u''_{jk} \int_{D_1} \rho_0 \approx u''_{jk} \bar{\rho} \Delta x \Delta z = \frac{\rho_1 + \rho_2}{2} u''_{jk} \Delta x \Delta z \tag{A-6}$$

and perform the integration on the right-hand side, remembering the continuity of $\bar{\mathbf{S}}$ along the horizontal interface, to get

$$\oint_{C_1} \bar{\mathbf{S}} \cdot \mathbf{n} = \int_{(x_0^+, z_0)}^{(x_0^+, z_0^+)} \bar{\mathbf{S}} \cdot (1, 0) + \int_{(x_0^+, z_0^+)}^{(x_0^-, z_0^+)} \bar{\mathbf{S}} \cdot (0, 1)$$

$$+ \int_{(x_0^-, z_0^+)}^{(x_0^-, z_0)} \bar{\mathbf{S}} \cdot (-1, 0) + \int_{(x_0^-, z_0)}^{(x_0^-, z_0^-)} \bar{\mathbf{S}} \cdot (-1, 0)$$

$$+ \int_{(x_0^-, z_0^-)}^{(x_0^+, z_0^-)} \bar{\mathbf{S}} \cdot (0, -1) + \int_{(x_0^+, z_0^-)}^{(x_0^+, z_0)} \bar{\mathbf{S}} \cdot (1, 0)$$

$$= \int_{z_0}^{z_0^+} S^2_{xx}\, dz \Big|_{x = x_0^+} + \int_{x_0^+}^{x_0^-} -S^2_{xz}\, dz \Big|_{z = z_0^+}$$

$$+ \int_{z_0^+}^{z_0} S^2_{xx}\, dz \Big|_{x = x_0^-} + \int_{z_0}^{z_0^-} -S^1_{xx}\, dz \Big|_{x = x_0^-}$$

$$+ \int_{x_0^-}^{x_0^+} -S^1_{xz}\, dz \Big|_{z = z_0^-} + \int_{z_0^-}^{z_0} S^1_{xx}\, dz \Big|_{x = x_0^+}$$

$$\approx S^2_{xx}(x_0^+, z_0) \frac{\Delta z}{2} + S^2_{xz}(x_0, z_0^+) \Delta x$$

$$- S^2_{xx}(x_0^-, z_0) \frac{\Delta z}{2} - S^1_{xx}(x_0^-, z_0) \frac{\Delta z}{2}$$

$$- S^1_{xz}(x_0, z_0^-) \Delta x + S^1_x(x_0^+, z_0) \frac{\Delta z}{2}$$

$$\approx (\lambda + 2\mu)_2 \frac{u_{j+1k} - u_{jk}}{\Delta x} \frac{\Delta z}{2}$$

$$+ \lambda_2 \frac{w_{j+1/2\,k+1} - w_{j+1/2\,k}}{\Delta z} \frac{\Delta z}{2}$$

$$+ \mu_2 \left(\frac{u_{jk+1} - u_{jk}}{\Delta z} + \frac{w_{j+1k+1/2} - w_{j-1k+1/2}}{2\Delta x} \right) \Delta x$$

$$- (\lambda + 2\mu)_2 \frac{u_{jk} - u_{j-1k}}{\Delta x} \frac{\Delta z}{2}$$

$$- \lambda_2 \frac{w_{j-1/2\,k+1} - w_{j-1/2\,k}}{\Delta z} \frac{\Delta z}{2}$$

$$- (\lambda + 2\mu)_1 \frac{u_{jk} - u_{j-1k}}{\Delta x} \frac{\Delta z}{2}$$

$$- \lambda_1 \frac{w_{j-1/2\,k} - w_{j-1/2\,k-1}}{\Delta z} \frac{\Delta z}{2}$$

$$- \mu_1 \left(\frac{u_{jk} - u_{jk-1}}{\Delta z} + \frac{w_{j+1k-1/2} - w_{j-1k-1/2}}{2\Delta x} \right) \Delta x$$

$$+ (\lambda + 2\mu)_1 \frac{u_{j+1k} - u_{jk}}{\Delta x} \frac{\Delta z}{2}$$

$$+ \lambda_1 \frac{w_{j+1/2\,k} - w_{j+1/2\,k-1}}{\Delta z} \frac{\Delta z}{2}, \tag{A-7}$$

where one-sided differences are used at the interface. We now equate equation (A-6) and equation (A-7) to give

$$u''_{jk} = \frac{1}{\tilde{\rho}}\left[\frac{(\lambda + 2\mu)_2 + (\lambda + 2\mu)_1}{2}\,\frac{u_{j+1k} - 2u_{jk} + u_{j-1k}}{\Delta x^2}\right.$$

$$+ \mu_2\,\frac{u_{jk+1} - u_{jk}}{\Delta z^2} - \mu_1\,\frac{u_{jk} - u_{jk-1}}{\Delta z^2}$$

$$+ \lambda_2\,\frac{w_{j+1/2k+1} - w_{j+1/2k}}{2\Delta x\Delta z} + \mu_2\,\frac{w_{j+1k+1/2} - w_{j-1k+1/2}}{2\Delta x\Delta z}$$

$$- \lambda_2\,\frac{w_{j-1/2k+1} - w_{j-1/2k}}{2\Delta x\Delta z} - \lambda_1\,\frac{w_{j-1/2k} - w_{j-1/2k-1}}{2\Delta x\Delta z}$$

$$- \mu_1\,\frac{w_{j+1k-1/2} - w_{j-1k-1/2}}{2\Delta x\Delta z}$$

$$\left. + \lambda_1\,\frac{w_{j+1/2k} - w_{j+1/2k-1}}{2\Delta x\Delta z}\right].$$

The u terms involving subscripts $j - 1/2, j + 1/2, k - 1/2$, and $k + 1/2$ are again approximated as in the text to maintain second-order accuracy.